Resolving and modeling the effects of Fe and Mn redox cycling on trace metal behavior in a seasonally anoxic lake

J. Hamilton-Taylor[1*], E.J. Smith[1], W. Davison[1] and M. Sugiyama[2].

[1]Environmental Science Department, Lancaster Environment Centre, Lancaster University, Lancaster, LA1 4YQ, United Kingdom

[2]Department of Environmental Sciences, Faculty of Integrated Human Studies, Kyoto University, Kyoto 606-8501, Japan

[*]corresponding author

REVISED MANUSCRIPT

5 NOVEMBER 2004

ABSTRACT

Vertical profiles of the dissolved and particulate (>0.45 μm) concentrations of Fe, Mn, Co, Ni, Cu, Pb, Al and Ba were determined on two occasions (14 and 22 August 1996) during summer stratification in a seasonally anoxic lake (Esthwaite Water, UK). The results were combined with contemporaneous in-situ measurements of water-column remobilization of the metals from settling particles at the base of the suboxic zone and other ancillary measurements. The combined data were interpreted with the aid of an equilibrium speciation model (WHAM6), incorporating metal-humic interactions and a surface-complexation description of binding to Fe and Mn oxides. The behavior of all the metals was related in different ways to the position of the O_2-H_2S interface and to Fe and Mn redox cycling. In the region of the O_2-H_2S interface the behavior of Co and to a lesser degree Ni was dominated by Mn redox cycling. Ba behavior was dominated by the biogenic precipitation and dissolution of barite and to a lesser degree by Mn redox cycling. The behavior of Al was linked to both Mn and Fe redox cycling, although the extent of binding to the oxides and to humic substances was poised with respect to pH. Unlike the other metals, the profiles of Pb and Cu showed little variation above the dissolved sulfide maximum, but modeling indicated that binding of Pb was significant to both Mn and Fe oxides. The featureless nature of the Cu profiles in the upper part of the water column was linked to its overriding association with dissolved humic substances. Below the dissolved sulfide maximum, Co, Ni, Ba, Cu, Pb and Mn were all affected by sulfide precipitation, probably through a common association with FeS. In the case of Co, Ni, Cu and Pb, inverse relationships between the measured dissolved and particulate concentrations were attributed to the coexistence of both filterable and nonfilterable FeS particles and associated mass balance effects. The observed behavior of the metals in relation to the role played by Fe and Mn oxides was generally consistent with WHAM6 predictions. The model predictions highlighted the fact that trace metal speciation in general, and binding to Mn and Fe oxides in particular, can be highly sensitive to the variations in solution conditions found in freshwater systems.

1. INTRODUCTION

High quality data sets of trace-metal distributions exist for a range of seasonally (Balistrieri et al. 1992; Hamilton-Taylor et al. 1996; Achterberg et al. 1997) and perennially (Balistrieri et al. 1994; Viollier et al. 1995) anoxic lakes, as well as for various anoxic marine basins (Jacobs and Emerson 1982; Kremling 1983; Jacobs et al. 1985). The overall picture of trace metal behavior in anoxic systems, however, can appear confused for a variety of reasons. The same metal can show different characteristics between systems. For example recent studies of Pb have reported a variety of distinctive concentration profiles, involving increased dissolved concentrations in suboxic or anoxic waters as a result of either Fe or Mn redox cycling (Benoit and Hemond 1990; Balistrieri et al. 1994; Balistrieri et al. 1995; Canfield et al. 1995; Viollier et al. 1995; Taillefert et al. 2000). In many cases these differences are likely to be real, reflecting variations in factors such as the availability of competing scavenging phases (e.g. Fe and Mn oxides, sulfides and organic matter) and the chemical composition of basin waters. With other metals the data appear contradictory. In the case of Cu an association with Fe and Mn oxides has been proposed on the basis of laboratory binding experiments and particle flux measurements (Baccini and Joller 1981; Sigg et al. 1995; Xue et al. 1997), whereas dissolved Cu profiles show few features other than lower concentrations below the oxic-anoxic boundary, due to sulfide precipitation, across the full range of anoxic-basin types (Baccini and Joller 1981; Jacobs and Emerson 1982; Kremling 1983; Jacobs et al. 1985; Balistrieri et al. 1992; Balistrieri et al. 1994; Xue et al. 1997). Another issue is an inability to separate the individual effects of redox cycling associated with Fe and Mn oxides, due to the overlapping nature of their distributions and the compressed depth scales of processes around the O_2-H_2S interface. For example significant increases in dissolved Ni with depth were observed around the interface in two meromictic lakes, but the relative roles of Fe and Mn redox cycling could not be distinguished (Balistrieri et al. 1994; Viollier et al. 1995). While it is becoming

increasingly clear that Co behavior is generally dominated by an association with Mn oxides across the full range of anoxic-basin types (Kremling 1983; Jacobs et al. 1985; Balistrieri et al. 1992; Balistrieri et al. 1994; Lienemann et al. 1997; Taillefert et al. 2002), previously in Esthwaite Water, the location of the present study, the effects of Fe and Mn redox cycling on Co could not be distinguished on the basis of profile characteristics alone (Achterberg et al. 1997).

The biogeochemical cycling of Ba in the open oceans has generated a great deal of interest in recent years, linked particularly to elucidating the nature of the processes resulting in the precipitation and dissolution of barite (Stroobants et al. 1991; Bertram and Cowen 1997). High concentrations of dissolved Ba in anoxic marine waters have been interpreted in terms of these same open-ocean processes (Kenison Falkner et al. 1993). The few existing freshwater studies indicate more complex Ba distributions that are poorly understood. The distribution of Ba has been linked to the redox cycles of either Fe (Viollier et al. 1995; Viollier et al. 1997) or Mn (Sugiyama et al. 1992; Sugiyama and Hori 1994) in different lakes, while in Esthwaite Water the observed Ba behavior during anoxia has been separately attributed to biogenic barite precipitation (Finlay et al. 1983) and the redox cycling of either Fe (Sholkovitz and Copland 1982) or Mn (Hamilton-Taylor et al. 1999).

The above examples demonstrate that the evidence linking trace-metal distributions to specific processes, particularly those involving Fe and Mn oxides, is often equivocal and basin-specific. It is also apparent that concentration profiles alone are generally not adequate to elucidate fully the complex processes controlling the cycling of trace metals in anoxic basins. The general aim of the present study is to provide new detailed insights into the biogeochemical cycling of Ba, Ni, Cu, Pb, Co and Al in a seasonally anoxic lake, particularly in relation to Fe and Mn redox cycling, through a unique multi-method approach. Water-column profiles of dissolved and particulate metal concentrations are combined with direct *in-situ* measurements of water column remobilization from settling particles, and the subsequent interpretation is supported by the

use of an equilibrium speciation model that includes different binding phases. The previously published remobilization measurements (Hamilton-Taylor et al. 1999) were made with a novel DGT-sediment trap device, developed during the course of the present study. The speciation model (WHAM6) (Lofts and Tipping 2001) combines an inorganic speciation code with a discrete-site, electrostatic sub-model of metal-humic interactions and a surface complexation description of the equilibrium adsorption of metals by various oxides. The model was run using its default database, calibrated on the basis of a large number of published binding experiments with isolated humic substances and preformed synthetic oxides. This approach therefore provides an effective test of the hypothesis that an equilibrium model, based on laboratory experiments and simple additive effects of the main binding phases, can provide an approximate description of *in situ* behavior.

Esthwaite Water (EW) is a biologically productive and seasonally anoxic UK lake that has been extensively studied in all aspects of limnology (Heaney et al. 1986). Previous EW studies include work on Fe, Mn and trace metals (Davison et al. 1980; Davison et al. 1982; Sholkovitz and Copland 1982; Hamilton-Taylor and Morris 1985; Hamilton-Taylor et al. 1996; Achterberg et al. 1997) that forms the basis of several reviews of redox cycling in lakes (Sholkovitz 1985; Davison 1993; Hamilton-Taylor and Davison 1995). The lake can therefore be regarded as a model system with well-defined limnological characteristics.

2. METHODS

2.1   Study Area, Field Measurements and Sampling

EW is situated in the English Lake District (54°22'N, 2°59'W). The lake has a surface area of 1.0 km^2, mean and maximum depths of 6.4 m and 15.5 m, a volume of 6.4 x 10^6 m^3, and a

typical hydraulic residence time of ~13 weeks. The sampling program corresponded to a period when summer stratification and seasonal anoxia were at their maximum stage of development.

The water-column profiling was undertaken on August 14 and 22 1996 at the deepest point in EW. Temperature and dissolved oxygen were measured *in situ* using a Clandon YSI Model 57 oxygen meter. For trace metals, 125-ml high density polyethylene (HDPE) sample bottles and all filtration and analytical equipment were pre-washed for 48 h in 10% Aristar HNO_3, rinsed in MilliQ (MQ) water, soaked for 24 hours in MQ water and rinsed for a second time in MQ water. Concentrated Aristar HNO_3 was added to each sample bottle in the laboratory, prior to sampling, sufficient to make the final sample pH $\simeq$ 2. All sampling equipment was transported to and from the field in polyethylene bags. Water samples were collected one at a time using a peristaltic pump and PVC tubing, and filtered on-line through 0.45 μm HAWP Millipore membrane filters held in Nuclepore filtration units. The complete sampling procedure took ~15 minutes per sample. The pump and tubing were flushed with 15 L of MQ water in the laboratory prior to fieldwork, and the filtration units were preloaded. At the start of each sampling day, an on-board field blank for trace metals was obtained by passing a 10 L MQ-water sample through the entire sampling procedure. The filters were subsequently retained in the filtration units and returned to the laboratory in polyethylene bags for particulate metal analysis.

Additional particulate-matter samples were collected and preserved under inert conditions on August 22, 1996, for redox-sensitive analysis in the laboratory. The sampling method involved pre-flushing a Nuclepore filtration unit, fitted with a Millipore polypropylene filter (0.6-μm pore size), with N_2-gas immediately before use. After filtration of ~200 ml of lake water, the connecting tubes to the filtration unit were sealed and the whole assembly immersed in liquid N_2.

Dissolved sulfide samples were collected on August 28 1996 using the same sampling-filtration methodology as for metals. The filtered water was passed directly into a 60-ml glass bottle, sealed with a Teflon-coated silicone rubber septum and aluminum cap. The dissolved

sulfide was fixed upon collection, as ZnS, by the addition of 4 ml of deoxygenated zinc acetate solution to the sampling bottle immediately prior to sample collection. Sulfide was determined colorimetrically in the laboratory, using an ethylene blue method (Davison and Lishman 1983).

2.2   Analytical Methods

The membranes used to filter the lake water samples on August 22 were digested in 0.002 M HNO_3 for 24 hours in order to obtain a direct measurement of labile particulate metal concentrations. The acid eluents were subsequently filtered through 0.45 μm HAWP Millipore membrane filters held in Nuclepore filtration units to remove undigested particles. The relative efficiencies of 0.002 M and concentrated HNO_3 (24-h leaches) for extracting Fe and Mn were recently compared in particulate samples from the oxic and anoxic zones of Priest Pot, a small, highly eutrophic lake, adjacent to EW (K. Warnken, pers. comm.). The comparison showed that the 0.002 M acid extracted ~70-80% of the conc. acid-leachable Mn in both oxic and anoxic samples. In the case of Fe, the dilute acid extracted a smaller fraction (20-25%) but the amounts leached by the two acids were highly correlated.

Following storage at 4°C for a maximum period of 5 weeks, the filtered acid eluents from the membrane digests and the filtered water samples were analyzed for Fe and Mn by electrothermal AAS (Perkin Elmer 4100ZL) and for Ba, Co, Al, Ni, Cu and Pb by ICP-MS (Varian Ultramass). Fifteen subsamples of MQ were analyzed to ascertain analytical detection limits of the metals (Table 1). All sample concentrations were above the detection limits and the field blanks.

Within 24-h of collection, the particulate samples that had been collected and stored under inert conditions for redox-sensitive analysis were transferred anoxically to the vacuum chamber of the Oxford Proton Microprobe (Grime et al. 1991) for analysis by MeV proton x-ray emission (PIXE) spectroscopy and proton- induced Rutherford backscattering spectroscopy (RBS). The 1-μm proton beam was rastered to obtain intensity maps, reflecting elemental masses per unit area

(i.e. mol cm^{-2}), from which elemental ratios and Pearson correlation coefficients were calculated. Other samples were transferred to a sealed tube in an H$_2$/N$_2$-filled glove box for analysis by electron spin resonance (ESR) spectroscopy, using a Bruker EMX instrument.

2.3   Chemical Speciation Modeling

WHAM6 (Lofts and Tipping 2001) combines the most recent versions of a series of published equilibrium speciation models written by Tipping and co-workers. WHAM6 is based on the earlier models, WHAM (Tipping 1994) and SCAMP (Lofts and Tipping 1998). WHAM6 includes an inorganic speciation code, a discrete-site electrostatic model of cation-humic interactions (Humic Ion-Binding Model VI) (Tipping 1998), and a surface complexation model of the equilibrium adsorption of cations by Mn, Fe(III), Si and Al oxides (Lofts and Tipping 1998). The model was used to predict the concentrations and hence fractions of each metal associated with colloidal or "dissolved" humic substances, Fe and Mn oxides, and particulate humic substances aggregated with the oxides (see below).

Representative conditions were used as input parameters rather than the detailed conditions at each depth and time. This approach allowed us to examine the effect of varying certain key parameters one at a time. The input parameters are given in Table 2. The major ion composition (Na, K, Ca, Mg, Cl and SO$_4$) was based on the long-term average concentrations in EW (Carrick and Sutcliffe 1982; Sutcliffe 1982) and the pH and alkalinity values on the detailed studies of Heaney et al. (1986) and Maberley (1996). EW is a circum-neutral lake with a background alkalinity of ~300 μequiv L^{-1}. During the summer the epilimnetic pH typically fluctuates between 8 and 9 due to a combination of high productivity, poor buffering, and the effects of weather conditions on mixing and stratification. Inorganic C is input to WHAM6 in the form of the partial pressure of CO$_2$. We therefore used partial pressures of CO$_2$ that produced an appropriate alkalinity at each pH value. The partial pressures (P_{CO_2}) are shown in Table 2, along with the

alkalinities subsequently computed. The corresponding CO_2 saturation values range from ~500%

in winter to ~5% at pH 9 in summer and are similar to those reported by Maberly (1996).

The concentration of dissolved humic substances in EW is typically within the range 1-2

mg L^{-1} (Tipping and Woof 1983).   Dissolved humic substances in surface freshwaters are

predominantly fulvic acid (Malcolm 1985), so the model simulations were run at 1 and 2 mg L^{-1}

fulvic acid for each set of pH and alkalinity conditions. Only the 2 mg L^{-1} results are reported in

detail because the computed differences were generally small. Two concentrations of Fe oxide,

equivalent to 0.7 and 30 μM particulate Fe, were used for the model simulations under summer

metalimnetic conditions, based on our own observations and those of Sholkovitz and Copland

(1982) and Davison et al. (1980) (see section 3.1). A single representative concentration

(equivalent to 0.5 μM particulate Mn) was used for Mn oxide (see section 3.1). Fe-oxide particles

in EW contain ~100 mg g^{-1} of humic substances, having the same uv-visible absorption

characteristics as the dissolved humics (Tipping et al. 1981). The Mn oxide formed in EW, in

contrast, contains only ~10 mg g^{-1} humic substances (Tipping et al. 1984). The WHAM6

simulations assumed these humic contents, as fulvic acid, in the Fe and Mn oxides (Table 2).

It has recently been suggested that Al and Fe(III) can compete significantly with trace

metals for binding by humic substances over a wide range of pH (4-9) (Tipping et al. 2002).

Dissolved Al was measured as part of the present study, while activities of Fe^{3+} ($a_{Fe^{3+}}$) were

estimated assuming equilibrium with Fe oxide, following the approach of Tipping et al. (2002).

Two values of the solubility product (i.e. $a_{Fe^{3+}}\big/a_{H^+}^3 = 10^{2.5}$ and $10^{4.0}$) were used, corresponding to a

range of possible Fe oxides. The choice of solubility product had a negligible effect on the

predicted speciation, and therefore the reported data were based on the value ($10^{4.0}$) that is more

appropriate to freshly precipitated Fe oxide (Tipping et al. 2002). The resulting Fe^{3+} activities,

calculated for the various pH values, are shown in Table 2. The total concentrations of Co, Ni, Ba,

Pb and Cu were each fixed at a single concentration, typical of the measured concentrations of

dissolved + labile particulate metal in the upper part of the water column, where the highest Fe and Mn-oxide concentrations were found. The concentration of Al was fixed at its typical dissolved concentration in the upper-water column, as labile particulate Al was not measured. The simulations were run with all trace metals present together.

3. RESULTS

3.1. General Water Column Conditions and Fe and Mn Distributions

The temperature and dissolved oxygen profiles (Fig. 1) show that summer stratification and seasonal hypolimnetic anoxia were well-established, although the detailed mixing conditions varied significantly between the two sampling dates. On August 14 some temperature stratification occurred throughout the upper part of the lake, whereas on August 22 there was a distinct well-mixed layer through the upper 4 m of the water column. These differences were also reflected in the dissolved oxygen profiles.

The observed vertical distributions of dissolved Fe and Mn (Fig. 2) were similar to those reported previously in EW (Davison et al. 1980; Davison et al. 1982; Hamilton-Taylor and Morris 1985; Hamilton-Taylor et al. 1996; Achterberg et al. 1997). The increase in dissolved Mn (i.e. Mn(II)) concentration at a shallower depth than that of dissolved Fe (i.e. Fe(II)) is due to the higher standard potential of the Mn redox reaction and the slower oxidation kinetics of Mn(II) (Davison 1993). The contrasting profile shapes for dissolved Fe (downward increasing) and Mn (approximately constant at depth) have been attributed to Mn being mainly supplied by reductive dissolution of its oxide within the water column, whereas dissolved Fe is mainly supplied from the sediments (Davison et al. 1980; Davison et al. 1982).

Labile particulate Fe and Mn both showed two maxima within the water column (Fig. 2). The depths of the upper peaks indicate that these maxima comprise mainly oxides, with the

10

shallower position of the Mn peak (5 m, compared to 7 m for Fe) again being consistent with the differences in the standard potentials and oxidation kinetics of the two metals. The ESR spectrum of the inertly preserved particulate sample from 7 m confirmed the dominance of Fe(III). The mimimum in particulate Fe at 10 m indicates that remobilization of the oxide was probably occurring in the anoxic water column at the time of sampling, as with Mn oxide. The magnitudes of the Fe- and Mn-oxide maxima of 0.7 µM Fe and 0.5 µM Mn (Fig. 2) can be compared with previously measured values for EW. Sholkovitz and Copland (1982) reported mid-water maxima of Fe and Mn oxides in August-early September of 5-20 µM Fe and 0.35-1.3 µM Mn. Davison et al. (1980) reported a mid-water Fe oxide concentration of 36 µM Fe in August 1977. These comparisons indicate that our own concentrations, obtained by digestion in 0.002 M HNO_3, provide a representative measure of the total Mn oxide concentrations, but may underestimate the total Fe oxide concentrations due to incomplete dissolution. This conclusion is consistent with the comparative study of leaching-agent effectiveness described in section 2.2. In the context of the WHAM6 simulations it should be noted that the peaks of both Fe and Mn oxides occurred within the metalimnion (see Figs. 1 and 2), where the pH is ~7 (see Section 2.3).

The intensely black color of the material comprising the lower (13 m) particulate-Fe peak (Fig. 2) suggests that it was substantially due to Fe sulfide. This interpretation is supported by the ESR and PIXE-RBS data. The ESR spectrum of the 13-m sample showed a much smaller intensity for Fe(III) than the 7-m sample, although the particulate Fe concentration was substantially greater at 13 m. The PIXE-RBS analysis of the 13-m particulate sample showed that Fe and S were the most abundant of the measured elements, apart from O, and that Fe correlated more closely with S than any other element. The correlation coefficient (r) between Fe and S was 0.90, while that between Fe and O was 0.12. The average molar ratio of Fe:S was 1:1.3, suggesting a stoichiometry close to that of the monosulfide. These characteristics contrasted with those of the 7-m sample, in which S was much less abundant and Fe and S showed no correlation ($r = -0.03$).

The dissolved sulfide profile was typical of EW during late-summer anoxia in showing a

characteristic maximum (Fig. 1) (Davison and Heaney 1978; Smith et al. 1996). It has been

demonstrated previously that equilibrium with respect to FeS precipitation exists below the

dissolved sulfide maximum, with the downward decreasing dissolved sulfide concentration being

linked directly to removal by FeS precipitation (Davison and Heaney 1978; Smith et al. 1996).

Examination of Figs. 1 and 2 shows that the magnitude of the peak of labile particulate Fe (~4.5

μM) at 13 m was similar to that of the decrease in dissolved sulfide below 10 m. This

approximately 1:1 inverse relationship is in line with the stoichiometry of FeS and suggests that the

trends in the two profiles below 10 m were affected by local mass balance between the dissolved

and labile particulate phases. A similar mass balance was not observed for dissolved Fe because of

its excess concentration. The maximum of particulate Mn at 13 m coincides with that of Fe (Fig.

2), suggesting a direct link with FeS precipitation. The nature of this relationship and similar

relationships for the trace metals are explored further in section 4.2.

3.2. Trace Metal Distributions

As a basis for interpretation, Pearson correlation coefficients (r) and simple linear

regressions were determined on various subsets of the data for the August-22 profiles. The

dissolved concentrations between depths of 6 and 10 m and the particulate concentrations between

3 and 10 m were used to elucidate the roles of Fe and Mn oxide precipitation-dissolution (see r

values in Table 3). The direct *in-situ* measurements of water column remobilization were made at

the base of the suboxic zone (at 7 m) in the period between the two sampling days in 1996 (14-22

August) and under similar redox conditions (at 4 m) between 12-14 August 1997 (Hamilton-Taylor

et al. 1999). The measured remobilization of trace metals was previously shown to be associated

with Mn oxide dissolution, and possibly release from unknown phases, but not to any significant

extent with Fe oxide dissolution (Hamilton-Taylor et al. 1999). The remobilization data are

presented in terms of metal:Mn ratios as a means of circumventing any problems associated with minor losses of dissolved metals from the DGT-trap devices by diffusion (Hamilton-Taylor et al. 1999). Comparisons are then made in Table 4 between these ratios and the gradients (Δmetal/ΔMn) obtained from the regression analysis.

The concentrations of dissolved Co and Ni increased with depth through the upper part of the anoxic zone, reaching distinct maxima at 10-12 m (Fig. 3). Above the maxima, their dissolved concentrations correlated well with both dissolved Mn and Fe (Table 3). Highly consistent Co:Mn molar ratios (0.26-0.29 x 10^{-3}) were obtained from the remobilization data and the regression analysis of the dissolved concentrations (Table 4), suggesting that Co behavior above 10 m was dominated by Mn cycling. Regression analysis of the dissolved concentrations between depths of 5.5 and 10 m in August 1991, taken from Achterberg et al. (1997), gives a similar Co:Mn ratio (0.32 x 10^{-3}), indicating its consistency over a number of years. Significant remobilization of Ni was also observed but, in contrast to Co, the various measures of the Ni:Mn ratio were highly variable (Table 4). The labile particulate Ni profile (Fig. 3) differed from that of Co in showing a distinct maximum in the oxic part of the water column at 4 m, 1 m above the Mn-oxide peak (Fig. 2).

The profiles of dissolved Ba and Al in August 1996 showed similar characteristics to those of Co and Ni through the upper part of the water column, but at depth generally exhibited a continuing downward increase instead of a maximum (Fig. 4). Between 6 and 10 m dissolved Ba and Al exhibited good correlations with both dissolved Fe and Mn (Table 3), but below 10 m correlated positively only with Fe (Table 5). Comparable dissolved Ba profiles in EW have previously been reported by Sholkovitz and Copland (1982) and McGrath et al. (1989). Labile particulate Ba exhibited a distinct maximum in the oxic part of the water column that coincided with the Mn-oxide peak at 5 m (Fig. 4 and Table 3). Substantial suboxic remobilization of Ba was measured by the trap device and the associated Ba:Mn ratio ~0.64 x 10^{-3} was similar in August

1996 and 1997 (Table 4). On the basis of the trap data, Hamilton-Taylor et al. (1999) argued that Mn oxide, but not Fe oxide, was an important and consistent source of the remobilized Ba. This conclusion is supported by microanalysis of individual oxide particles from EW that showed measurable Ba in Mn oxide, but not in Fe oxide (Tipping et al. 1981; Tipping et al. 1984). However, a comparison of the Ba:Mn ratios, derived from the DGT-trap measurements and from the regression analysis, shows a clear sequence (Table 4): DGT-trap < dissolved metal regression < labile particulate metal regression. This variability, combined with the lack of correlation between dissolved Mn and Ba below 10 m, indicates that processes additional to Mn redox cycling also play an important role in the observed behavior of Ba.

As with Ba a substantial amount of suboxic remobilization of Al was measured by the trap device and the associated Al:Mn ratio was 3-times higher in 1997. The trap-derived Al:Mn values encompass the value derived from regressing the dissolved concentrations between 6 and 10 m (Table 4), suggesting that Mn cycling was capable of accounting for much of the accumulated dissolved Al over this depth interval. However, because all of the Mn oxide is generally remobilized in the water column of EW during mid-summer, with no significant diffusive input from the sediments (see Fig. 2 and section 3.1), the Mn redox cycle cannot explain the steadily increasing downward concentration of dissolved Al below 10 m (cf. Figs. 2 and 4). The overall shape of the profile therefore suggests that the behavior of Al may also be linked to the Fe redox cycle.

The profiles of dissolved Pb and Cu were relatively featureless, except for a single high-Pb concentration at mid-depth and a poorly-defined decrease in dissolved Cu from ~10 nM in surface waters to <5 nM in deep waters (Fig. 5). The lowest dissolved Cu concentrations occurred in the region of the Fe-sulfide maximum between 11 and 14 m. The dissolved Cu profiles were similar to those observed in August and September 1991 by Achterberg et al. (1997). Labile particulate Pb and Cu both showed small maxima at 4 m that coincided with that of Ni. The maxima were

possibly linked to their position at the base of the well-mixed layer as a result of some sort of sedimentation control (Kleeberg and Schubert 2000). No measurable Pb or Cu remobilization was observed in the DGT-trap device in 1996 and they were not determined in 1997 (Smith 1998). Thus there was no observational evidence that Pb and Cu were linked to the redox cycles of either Fe or Mn above a depth of 10 m.

The labile particulate concentrations of Mn, Co, Ni, Ba, Pb and Cu were all highly correlated with that of Fe between 10 and 15 m on August 22 (Table 5), indicating that the six metals were also associated with sulfide precipitation. The dissolved-concentration profiles of sulfide, Co, Ni, Pb and Cu also covaried between 10 and 15 m on August 22 (Figs. 1, 3 and 5) and showed inverse relationships with their corresponding particulate concentrations. The inverse relationship was best developed for Co and Ni. The gradients of their dissolved-versus-particulate regression lines between 11 and 15 m were –0.8 and –1.1, respectively, suggesting good mass (strictly concentration) balances between the measured particulate and dissolved fractions. There was a similar mass balance between dissolved sulfide and particulate Fe (see section 4.2), and approximate mass balances for Cu and Pb. These mass balances could only be observed because the dissolved and particulate concentrations were similar. In the case of Fe, Mn and Ba, such effects were either absent or not apparent because of the predominance of the dissolved concentrations.

4. DISCUSSION

4.1 Model Predictions

In general agreement with observations, WHAM6 predicts that dissolved trace-metal concentrations predominate over those associated with Fe and Mn oxides for all metals except Pb (Table 6). The dissolved fraction in the context of the modeling results refers to the sum of the

true solution and colloidal fulvic acid fractions, where the amount in true solution comprises the free metal ion plus inorganic complexes. Most of the Co is predicted to be in true solution with Mn oxide accounting for 5-19% of the total Co. The predicted values of the Co:Mn ratio (0.2-0.7 x 10^{-3}), resulting from Co adsorption to Mn oxide, encompass the observed range of values (0.26-0.32 x 10^{-3}). WHAM6 predicts that Fe oxide-bound Co increases to 3% of the total at the higher Fe oxide concentration (30 μM Fe), but it remains subordinate to the Mn-oxide fraction. The predicted Co:Fe ratio (2 x 10^{-6}) of the Fe oxide in this scenario is two orders of magnitude less than the corresponding Co:Mn ratio, highlighting the relatively low affinity of Co for Fe oxide. The good agreement between the model predictions and field observations, obtained over several years, provides strong evidence in support of Mn oxide dissolution being the predominant source of dissolved Co in EW under reducing conditions.

Most of the Ni is predicted to be in true solution, although as much as 10% of the total Ni is complexed by colloidal fulvic acid (Table 6). At the measured concentration of Fe oxide (0.7 μM Fe), Ni adsorbed to Fe and Mn oxides is predicted to be present at low levels (≤1% of the total Ni) (Table 6). A trend is apparent in the predicted oxide fractions of Ni at 0.7 μM Fe in that at pH 7, typical of waters in the vicinity of the oxide maxima, Mn oxide is more important than Fe oxide, whereas at pH 9, typical of the well-mixed surface waters in summer, Fe oxide is more important. Since the zero point of charge of amorphous Fe oxide and goethite is around pH 8 (Stumm and Morgan 1996), the effect of electrostatics on binding is probably the main cause of this predicted pH trend. At the upper limit of possible Fe oxide concentrations (30 μM Fe), the Fe oxide fraction may become more important than Mn oxide even at pH 7 (Table 6). The predicted Ni:Mn ratio, resulting from adsorption to Mn oxide, is 0.1 x 10^{-3} at the likely pH (7) at the Mn oxide peak, but decreases to 0.02 x 10^{-3} at pH 9. Therefore, despite the low absolute level of predicted Ni binding to Mn oxide, it is enough to account for the remobilization of Ni, measured by the DGT-trap device in 1996, and is close to the Ni:Mn ratio derived from regressing the dissolved concentration

data (Table 4). On the other hand, the predicted Ni:Mn values fall well below the values derived

from regressing the labile particulate data and from the observed trap remobilization in 1997

(Table 4). The corresponding predicted Ni:Fe values, resulting from Ni adsorption to Fe oxide,

vary between 1 x 10^{-5} at pH 7 and 7 x 10^{-5} at pH 9. These values are too small for the measured

particulate Fe-oxide concentrations (max. 0.7 µM Fe) to make a significant contribution to the 1-

nM particulate Ni peak at 4 m or to the measured DGT-trap remobilization. The combined field

and modeling results thus indicate that the redox cycling of Mn, but not Fe, has an observable

effect on the vertical concentration profile of dissolved Ni and its remobilization in the vicinity of

the oxic-anoxic boundary. At the same time, the varying Ni:Mn values indicate that its behavior is

more complex than that of Co and is probably affected by additional processes. The EW

observations provide some of the clearest evidence of a link between Mn redox cycling and Ni in

anoxic basins, although a Ni-Mn link was also suggested by the dissolved-concentration profiles in

another seasonally anoxic lake (Balistrieri et al. 1992).

More than 99% of the dissolved Ba is predicted to be in true solution in all simulations

(Table 6). Adsorption of Ba to Mn oxide is predicted to be more important than to Fe oxide,

although particulate fulvic acid, associated mainly with the Fe oxide, becomes the main particulate

fraction of Ba at the upper limit of possible Fe oxide concentrations (30 µM Fe) (Table 6). The

predicted Ba:Mn ratio, due to Ba adsorption to Mn oxide, is more or less constant in all model

simulations at ~0.02 x 10^{-3}. This value is more than 30-times less than the lowest of the values

obtained from the field data (Table 4). Tipping et al. (1984) also reported that the levels of Ba in

Mn oxide particles in EW were high relative to those expected from adsorption to a pre-formed

phase. They interpreted this as indicating incorporation into the oxide during formation. Another

possible explanation is an inappropriate binding constant in WHAM6 for Ba uptake by Mn oxide.

The default constant was derived from a linear-free energy relationship, due to the lack of

published experimental data for Ba binding to Mn oxide (Lofts and Tipping 1998). Sugiyama et

al. (1992) also noted exceptionally strong binding of Ba to Mn oxides in Lake Biwa, and associated binding experiments yielded a distribution coefficient for Ba that was an order of magnitude or more greater than that of other alkaline earth elements. The corresponding Ba:Fe values, predicted by WHAM6 as a result of Ba adsorption to Fe oxide, vary between 3×10^{-6} at pH 7 and 6×10^{-6} at pH 9. These low values suggest that Fe redox cycling makes no significant contribution to the observed water-column behavior of Ba.

WHAM6 predicts that the distribution of Al between true solution and colloidal fulvic acid is very sensitive to pH in EW (Table 6). At pH 7 Al is associated mainly with fulvic acid, whereas at pH 8-9 it is predominantly in true solution due to the increasing importance of $Al(OH)_4^-$. The model also predicts that the fractions of Al adsorbed by Mn and Fe oxides decrease sharply with increasing pH, again due to $Al(OH)_4^-$, while the relative importance of Fe rather than Mn oxides increases (Table 6). Generally, the particulate fulvic-acid fraction associated with each oxide is predicted to contain more than the oxides themselves. The exception to this generalization is that at the pH (7) of the oxide maxima in the metalimnion, more than 80% of the Al bound by Mn oxide is predicted to be associated with the pure oxide. The predicted overall Al:Mn ratio of this oxide at pH 7 is 2×10^{-3} and 0.5×10^{-3} at 1 and 2 mg L^{-1} colloidal fulvic acid, respectively. These values are of a similar magnitude to the values derived from the DGT-trap data and from regression analysis of the dissolved Al and Mn concentrations between 6 and 10 m (Table 4). In contrast, the predicted Al:Mn values at higher pH (e.g. 5×10^{-7} at pH 9, 2 mg L^{-1} colloidal fulvic acid) are orders of magnitude lower than the values shown in Table 4. It follows that adsorption of Al to Mn oxides is sufficient to account for the levels of Al remobilization observed around the oxic-anoxic interface as a result of Mn redox cycling. The highly pH-dependent nature of Al adsorption to Mn oxide probably contributes to the variable Al:Mn ratio obtained from the field measurements (Table 4), especially given the extent of pH variation with time and depth during the summer period. The reverse argument may explain why the measured Co:Mn ratios were so

constant (Table 4). The predicted Co:Mn ratio due to adsorption by Mn oxide varies by a factor

of only ~3 between pH 7 and 9, so is much less sensitive to the known pH variations. As the

degree of pH dependency of Ni binding to Mn oxide is predicted to be intermediate between that

of Co and Al, it may contribute to the observed Ni:Mn variability (Table 4).

The predicted Al:Fe values at the pH (7) of the Fe oxide peak, associated with adsorption,

are 2×10^{-3} and 1×10^{-3} at 1 and 2 mg L^{-1} fulvic acid, respectively. These values agree with the

Al:Fe ratio (2.1×10^{-3}), derived from regressing the dissolved Al and Fe data below 10 m on

August 22. At higher pH the predicted Al:Fe values are much lower (e.g. $\sim 10^{-4}$ at pH 8 and 10^{-6} at

pH 9). The model predictions therefore support the field data in indicating that the observed

behavior of Al in EW is linked to the redox cycling of both Mn and Fe, although in the case of Fe

it probably occurs mainly through an association with the organic fraction of the oxide. An

association between Fe oxide and Al in lake sediments was previously reported by Fortin et al.

(1993).

WHAM6 predicts that the dissolved-Pb fraction increases between pH 7 and 9 from 16% to

79% of total Pb at the measured Fe-oxide concentration and 2 mg L^{-1} fulvic acid (Table 6). These

predictions are reasonably consistent with the observations in that a substantial proportion of Pb

(~25%) was in the labile particulate fraction. The dissolved Pb is predicted to be dominantly

complexed by colloidal humic substances with <1 % in true solution. The simulations also

indicate that both oxides are likely to contain substantial amounts of Pb, with Mn oxide being

relatively more important at pH 7 and Fe oxide at higher pH. At the upper limit of possible Fe

oxide concentrations (30 μM Fe), the Fe oxide fraction is predicted to dominate even at pH 7

(Table 6). The particulate fulvic fractions of the oxides are relatively unimportant in all cases.

The model simulations highlight a feature that differentiates Pb from the other trace metals. In the

latter case, the metal:Mn and metal:Fe ratios of the respective oxides are largely independent of the

oxide concentrations, e.g. the change from low (0.7 μM Fe) to high (30 μM Fe) Fe-oxide

concentration has a negligible effect on the ratios. This is because the trace metals are predominantly in solution, so that changes in the particulate metal fractions at varying oxide concentrations have a negligible effect on the dissolved concentrations. In the case of Pb, significant competition effects are predicted because of the high affinity of both oxides for the metal. Other natural solids are likely to have similar competition effects due to the high particle affinity of Pb generally. This affinity probably accounts for the absence of any measurable Pb remobilization in the DGT-trap device and the limited increase in dissolved Pb below the oxic-anoxic boundary. Thus when Mn oxide and its associated Pb were remobilized in the traps, Pb was probably re-adsorbed by the Fe oxide and other natural particles, rather than being taken up by the DGT device to any measurable extent. A similar Pb re-adsorption effect was observed following the selective removal of Mn oxide in a sequential chemical extraction of a natural mixture of Fe and Mn oxides (Tipping et al. 1985).

The model predicts that Cu is mainly in solution as the fulvic complex, irrespective of pH and fulvic concentration (Table 6). Most of the remaining Cu is associated with the particulate fulvic material, more than 90% of which is associated with the Fe oxide. In terms of the pure oxides, more Cu is bound by Fe rather than Mn oxide. At the likely pH (7) of the Mn oxide peak, the predicted Cu:Mn ratio due to adsorption by Mn oxide and its associated particulate fulvic acid is ~1 x 10^{-5}. This ratio is equivalent to 0.005 nM particulate Cu being associated with the Mn oxide peak at 5 m and to 0.5 nM dissolved Cu being associated with the increase in dissolved Mn between 6 and 10 m. These concentrations are negligible compared with the observed concentrations of particulate and dissolved Cu (Fig. 5). Furthermore the predicted ratio is about an order of magnitude less than could be detected by the DGT-trap device (Hamilton-Taylor et al. 1999). A similar situation exists with respect to the Fe profiles, although the increased dissolved Fe below 10 m would be associated with an increase in dissolved Cu of ~5 nM, based on a predicted Cu:Fe ratio of ~5 x 10^{-5}. Such an increase was probably masked by the effects of sulfide

precipitation. The model predictions are therefore consistent with the field observations in suggesting that Mn redox cycling is unimportant for Cu in EW, while Fe redox cycling has no observable effects on Cu profiles other than those due to sulfide precipitation. The absence of any observable Cu cycling in the sub-oxic region of EW, and probably other anoxic basins, is due in large part to the overriding effect of complexation by humic substances.

4.2 Sulfide Precipitation

Formation of the solid phase(s) responsible for the maxima of particulate metals at 13 m could be controlled by the solubility of individual metal sulfides or an association with the major FeS phase. WHAM was modified to include the metal-sulfide stability constants quoted in Huerta-Diaz et al (1998) and used to calculate the saturation index with respect to each metal sulfide. The results were similar to those reported for other anoxic basins in showing a high degree of variation in the calculated saturation indices (Jacobs et al. 1985; Balistrieri et al. 1992; Balistrieri et al. 1992; Balistrieri et al. 1994), ranging from undersaturation with respect to Mn sulfide and α NiS to a large degree of oversaturation for Cu and Pb sulfides. This variability in the extent of saturation weakens the argument for the coincident peaks in particulate concentrations being due to formation of individual sulfides and favors instead an association between the trace metals and FeS. Davison et al. (1992) reported 4000 ppm Cu in FeS-rich particles in EW, which is equivalent to an atomic Cu:Fe ratio of 5 x 10^{-3}. The Cu:Fe ratio obtained from the particulate maxima at 13 m was also 5 x 10^{-3}. Coprecipitation and adsorption of Co, Ni and Mn by FeS has previously been demonstrated in the laboratory under conditions typical of anoxic waters (Arakaki and Morse 1993; Morse and Arakaki 1993), while Mn scavenging by FeS in Esthwaite Water was previously suggested on the basis of laboratory experiments (Hamilton-Taylor et al. 1996).

Despite the evidence presented above it is not easy to explain the well-defined solid-solution partitioning of the metals observed between 10 and 15 m, in particular the apparent mass-

balance effects, in terms of control by sulfide precipitation, coprecipitation or adsorption by FeS. The observed similarity in behavior of such a chemically diverse range of metals suggests that there is a single controlling mechanism. We hypothesize that Mn, Ba, Co, Ni, Cu and Pb were associated with FeS particles in the sub-micron to micron size range. Accordingly the nonfilterable fraction would contain colloidal as well as truly dissolved metal. Aggregation or particle growth, with resulting conversion of some fraction of the particles from a nonfilterable to a filterable size (0.45-μm pore size), could then account for the particulate maxima at around 13-m depth. The mass balance effect between "dissolved" and "particulate" phases for Co, Ni, Cu, Pb and sulfide simply reflects this transfer. The profiles of nonfilterable Mn and Ba were, in contrast, unaffected because of the high concentrations in true solution.

The apparent mass balances suggest that vertical transport of Co, Ni, Cu and Pb was relatively unimportant compared to transfer between colloidal and particulate phases. The low, implied settling rate for FeS particles is consistent with independent observations of their size. Previous PIXE-RBS analysis has shown that FeS particles in EW are not resolvable with a 1-μm proton beam (Davison et al. 1992). Mackinawite particles formed in laboratory experiments were found to be greater or less than 0.1 μm, depending on solution conditions and the associated degree of supersaturation (Arakaki and Morse 1993; Morse and Arakaki 1993). Mackinawite is a metastable Fe sulfide that readily forms from amorphous FeS (Rickard 1989; Morse and Arakaki 1993). In anoxic waters in Framvaren Fjord, twice the mass of FeS particles was collected by filtration through 0.2-μm filters, compared with that obtained using 0.4-μm filters (Jacobs et al. 1985). Clearly the commonly used pore sizes of membrane filters (0.2 to 0.45 μm) lie within the typical size range of FeS particles, so that the conversion of nonfilterable to filterable FeS observed in EW was quite probably associated with a relatively small increase in particle size. Estimation of the settling rates of the particles, using Stokes Law and assuming a density of 3 g cm^{-3}, gives values in the order of 10^{-3} and 10^{-1} m day^{-1} for particles of 0.1 and 1-μm diameter,

respectively. These rates are consistent with approximate elemental mass balances being

maintained for periods of days given the 1-m sampling intervals.

If the FeS particles and their associated trace-metal contents are distributed between

colloidal and filterable fractions, there will be an effect on the distribution coefficient (K_d in L kg^{-1})

of each metal. K_d values were calculated for depths between 11 and 15 m, using Equation 1, where

M_p is the particulate (filterable) metal concentration (mol L^{-1}), [FeS] is the "particulate FeS"

concentration (kg L^{-1}) based on the measured particulate Fe, and M_d is the dissolved (nonfilterable)

metal concentration (mol L^{-1}).

$$K_d = \frac{\dfrac{M_p}{[FeS]}}{M_d} \qquad \qquad \textbf{Equation 1}$$

The calculated K_d values for Co, Ni and Cu decrease with increasing M_d, while the values for Mn

and Ba remain relatively constant (Fig. 6a). The K_d values for Pb were relatively noisy and are

omitted. The observed K_d trend for Co, Ni and Cu reflects the mass balance effect, i.e. M_p

increased as M_d decreased. The numerator in Equation 1 (M_p/[FeS]) remained relatively constant,

reflecting the good correlations of particulate trace metal concentrations with that of Fe.

Values of K_d were simulated while varying the proportion of metal in colloidal and

particulate forms. Simplifying assumptions were that throughout the 10-15 metre zone: (1) there is

a constant background concentration of truly dissolved trace metal (M_b); and (2) the total

concentration of trace metal associated with particulate and colloidal FeS (M_{FeS}) is constant. It

follows from these assumptions that the total trace metal concentration ($M_b + M_{FeS}$) is also

constant throughout the 10-15 metre zone and this was approximately the case. The simulated

concentration of particulate (filterable) metal, sim-M_p, simply reflects the fraction of Fe present in

the particulate form (Equation 2).

$$\text{sim-}M_p = M_{FeS}\,\frac{Fe_p}{\text{max-}Fe_p} \qquad \qquad \textbf{Equation 2}$$

where max-Fe_p is the maximum Fe concentration (4.5 µM) associated with particulate (filterable) FeS. Four typical values of particulate (filterable) Fe concentrations in the anoxic zone (Fe_p = 1, 1.5, 3, 4.5 µM) were chosen to provide a range of colloid to particulate ratios. The simulated concentration of dissolved (filterable) metal, sim-M_d, is the sum of the truly dissolved metal and the metal present associated with colloidal FeS (Equation 3).

$$\text{sim-}M_d = M_b + M_{FeS} - \text{sim-}M_p \qquad\qquad \textbf{Equation 3}$$

The M_{FeS} and M_b values used in the calculations (Table 7) were based on the observed concentrations. The terms sim-M_p and sim-M_d were then combined with [FeS], derived from the four Fe_p values, to calculate K_d using Equation 1 (Fig. 6b). Comparability with the observed K_d values is good, demonstrating that the assumption of metals associated with FeS particles being present in colloidal and particulate form is consistent with the data. The observed log K_d values are plotted against log [FeS] in Fig. 6c. Although the trends are not so clear as those against M_d, there is a tendency for K_d to increase with [FeS] for most metals. This trend is the opposite of the "particle concentration effect" normally observed in aquatic systems in which colloids have an important role (Honeyman and Santschi 1988; Honeyman and Santschi 1989).

Other than the Framvaren Fjord study, cited above, field evidence for the existence of colloidal FeS is scarce. Colloidal sulfides were considered as possible explanations of some observed trace metal behavior (Benoit and Hemond 1990; Taillefert et al. 2000) but, apart from electrochemical evidence for a dissolved multi-nuclear FeS species (Davison et al. 1998), we found only one study with direct evidence of colloidal sulfides in lakes (Viollier et al. 1997). Balistrieri et al. (1994) observed maxima of particulate (>0.4 µm) Cu, Pb, Zn and Ni below the dissolved sulfide maximum in a meromictic lake that coincided with dissolved minima of the same metals, approximately on a 1:1 basis for each metal. The relationships are similar to those observed in EW that we have interpreted in terms of mass balances between colloidal and particulate sulfides.

4.3 Biogeochemical Cycling of Ba and Al

Studies of Ba and Al in anoxic basins are scarce in comparison with those of Co, Ni, Pb and Cu. The combined observational and modeling results indicated that the behavior of Ba in EW was associated with the redox cycle of Mn, but not Fe, plus at least one additional process. Finlay et al. (1983) previously showed that the distribution of Ba in EW is affected by the use of barite as an intracellular gravity sensing mechanism by the ciliated protozoan, *Loxodes*. We suggest that the behavior of Ba in the present study, including the observed sequence of Ba:Mn values (DGT-trap < dissolved metal regression < labile particulate metal regression), can be explained by a combination of the Mn redox cycle and barite precipitation-dissolution associated with *Loxodes*. The relationship between the Ba:Mn ratio calculated from the DGT-trap measurements (0.64×10^{-3}) and the particle-derived ratio (13.7×10^{-3}) indicates that Mn oxide accounts for only a small fraction (5%) of the observed particulate-Ba maximum at 5 m. Finlay et al. (1983) showed that the abundance of *Loxodes* peaked immediately above the oxic-anoxic boundary in EW and also correlated with a 7-nM peak of particulate Ba. They independently estimated that 5.5 nM of this was due to *Loxodes*. This estimate can be compared with the 6.4-nM peak of labile particulate Ba seen at 5 m in Fig. 4. Given the difference in the Ba:Mn ratios derived from the DGT-trap measurements and the particle-based regression analysis, it follows that the particulate-Ba maximum at 5 m was also due mainly to the presence of *Loxodes*. Whether its coincidence with the Mn oxide peak is fortuitous or whether there is a tighter coupling of the two processes (e.g. Mn oxidizing bacteria acting as a food source for *Loxodes*) is unknown. The continuing small increase in dissolved Ba concentrations below 10 m (Fig. 4) is probably linked to the further dissolution of the microbial barite in bottom sediments. The accumulated evidence gives no support for an association of Ba with Fe cycling in EW, as originally suggested by Sholkovitz and Copland (1982) on the basis of correlations between the seasonal and depth distributions of the two metals.

In relation to the observed binding of Ba to FeS, database searching has failed to find any previous report of a Ba-sulfide association in either lake or marine anoxic basins. The association probably arises through adsorption, as with Mn (Arakaki and Morse 1993). Other group 2 metals (Ca and Mg) adsorb to mackinawite to a similar extent to Mn (Morse and Arakaki 1993), and Fig. 6 shows that the observed K_d values of Ba and Mn were similar.

The profiles of dissolved Ba concentrations in EW are most like those in the Cariaco Trench and Framvaren Fjord (Kenison Falkner et al. 1993) in showing downward increasing concentrations, commencing slightly above the O_2-H_2S interface. In Pavin Lake, a meromictic water body, the main increase in dissolved Ba occurred in the lower part of the anoxic zone in the region of the water-sediment interface (Viollier et al. 1995). The particulate Ba profile showed a maximum immediately above the O_2-H_2S interface, that correlated better with the Fe-oxide peak than that of Mn oxide, and a bottom maximum. These maxima were interpreted as being due to scavenging by Fe(III) oxide and ferrous phosphate, respectively (Viollier et al. 1997). We suggest that biogenic barite cannot be discounted as a possible source of the mid-depth maximum, the magnitude of which (~5 nM) was the same as that at 5 m in EW.

The distribution of Al in EW is similar to that observed in Pavin Lake (Michard et al. 1994; Viollier et al. 1995) in that dissolved Al concentrations and pH are high in surface productive waters and low in the underlying region of Mn and Fe-oxide formation. The dissolved Al profile in Pavin Lake was attributed to the effects of pH on $Al(OH)_3$ solubility (Viollier et al. 1995). Saturation conditions with respect to $Al(OH)_3$ in EW were determined by using WHAM6 to calculate the ion activity product (IAP = $a_{Al^{3+}} / a_{H^+}^3$) over a range of typical conditions (Table 8). The pH values were taken from Heaney et al. (1986), fulvic acid concentrations from Tipping and Woof (1983), and the total dissolved Al concentrations from Fig. 4. The solubility product of $Al(OH)_3$ is reported to be in the range 10^8-10^9 (LaZerte 1989). The waters are therefore undersaturated throughout the epilimnion and metalimnion and approach saturation only in anoxic

hypolimnetic waters. Most significantly the metalimnetic waters in the region of the Mn and Fe oxide maxima on August 22 are around an order-of-magnitude undersaturated with respect to the least soluble form of $Al(OH)_3$, so that $Al(OH)_3$ precipitation cannot be the cause of the dissolved Al minimum at 6 m (see Figs. 1, 2 and 4). The calculation of $Al(OH)_3$ saturation in the hypolimnion excluded Al-sulfide species, since no stability constants were found in either the Smith and Martell (1976) or NIST (1997) databases. Overall the data are inconsistent with control by $Al(OH)_3$ solubility and further support the role played by Fe and Mn redox cycling. Because the dissolved Al concentrations are around 5-times lower in Pavin Lake than in EW, while the pH values and DOC concentrations are broadly similar, we speculate that Fe and Mn redox cycling may also affect the behavior of Al in this meromictic lake.

4.4 General Discussion

The results of the WHAM6 modeling are generally consistent with the field observations made under oxic and suboxic conditions in EW. In particular, the model provides a good prediction of the observed binding of Co and Ni to Mn oxide and of Al to both Mn and Fe oxides. The excellent agreement between the observed and predicted Co:Mn ratios appears surprising given that Co binding to Mn oxide can involve substitution in structural sites and oxidation to Co(III) (Crowther et al. 1983). However, while the experimental binding data are described by surface complexation within WHAM6, the underlying binding mechanisms occurring in the experiments may in reality be more complicated. For example the data set used to calibrate Co binding in WHAM6 involved a 48-h sorption period that resulted in structural substitution of Co for Mn, in addition to surface exchange (Loganathan and Burau 1973). More generally, however, the degree to which trace metal binding to Fe and Mn oxides is predicted by an equilibrium model based on adsorption to preformed synthetic phases was unexpected, given the complex, dynamic and often microbial nature of processes in lakes. The model has proved a valuable tool in

evaluating this field data set. Given the inherent simplifications of WHAM6 and the input data used in the modeling, including the omission of other adsorbents (e.g. clay minerals and silica) and organic ligands of microbial origin (Sigg et al. 1995; Ellwood et al. 2001), further testing of the model against other field-data sets is required before it can be used more generally for predictive purposes.

The geochemical modeling highlights the fact that trace metal speciation in general, and binding to Mn and Fe oxides in particular, can be highly sensitive to the variations in solution conditions occurring through a depth-interval of just a few metres in a typical lake. It follows that the relative and absolute importance of Mn and Fe oxides as trace-metal carriers will vary greatly over the full range of freshwater conditions. Conversely, we suggest that it is no coincidence that the metal (Co) showing the most consistent behavior in both freshwaters and seawater is the metal predicted by WHAM6 to be the least sensitive to variations in solution conditions.

5. CONCLUSIONS

The dissolved and particulate concentration profiles and the water-column remobilization of Co, Ni, Ba, Al, Cu and Pb in EW during midsummer anoxia showed distinctive patterns of behavior for each metal that were related to the position of the O_2-H_2S interface and to Fe and Mn redox cycling. In the region of the O_2-H_2S interface, the behavior of Co and to a lesser degree Ni was dominated by Mn redox cycling. Ba behavior was dominated by the biogenic precipitation of barite, mediated by protozoa, and its subsequent dissolution, and to a lesser degree by Mn redox cycling. The behavior of Al was linked to both Mn and Fe redox cycling, but the extent of binding to Mn and Fe oxides and to humic substances was poised with respect to pH. The profiles of Pb and Cu showed comparatively little variation above the dissolved sulfide maximum, even though, in the case of Pb, the WHAM6 simulations indicated that binding to Mn and Fe oxides was

important. The featureless nature of the Pb profiles in the upper part of the water column was linked to its tendency to bind to all particle types and to dissolved humic substances, whereas that of Cu was linked to its overriding association with dissolved humic substances. Below the dissolved sulfide maximum, Co, Ni, Ba, Cu, Pb and Mn were affected by sulfide precipitation, probably through a common association with FeS. In the case of Co, Ni, Cu and Pb, inverse relationships between the measured "dissolved" and particulate concentrations were attributed to size differences in the FeS particles, i.e. nonfilterable and filterable by 0.45-μm membrane filters.

ACKNOWLEDGMENTS

REFERENCES

Achterberg, E. P., C. M. G. van den Berg, M. Boussemart and W. Davison (1997). Speciation and cycling of trace metals in Esthwaite Water: A productive English lake with seasonal deep-water anoxia. *Geochim. Cosmochim. Acta 61*, 5233-5253.

Arakaki, T. and J. W. Morse (1993). Coprecipitation and adsorption of Mn(II) with mackinawaite (FeS) under conditions similar to those found in anoxic sediments. *Geochim. CosmochIM. Acta 57*, 9-14.

Baccini, P. and T. Joller (1981). Transport processes of copper and zinc in a highly eutrophic and meromictic lake. *Schweizerische Zeitschrift für Hydrologie - Swiss Journal of Hydrology 43*, 176-199.

Balistrieri, L. S., J. W. Murray and B. Paul (1992). The biogeochemical cycling of trace metals in the water column of Lake Sammamish, Washington: Response to seasonally anoxic conditions. *Limnol. Oceanogr. 37*, 510-528.

Balistrieri, L. S., J. W. Murray and B. Paul (1992). The cycling of iron and manganese in the water column of Lake Sammamish, Washington. *Limnol. Oceanogr. 37*, 510-528.

Balistrieri, L. S., J. W. Murray and B. Paul (1994). The geochemical cycling of trace elements in a biogenic meromictic lake. *Geochim. Cosmochim. Acta 58*, 3993-4008.

Balistrieri, L. S., J. W. Murray and B. Paul (1995). The geochemical cycling of stable Pb, ^{210}Pb, and [210]Po in seasonally anoxic Lake Sammamish, Washington, USA. *Geochim. Cosmochim. Acta 59*, 4845-4861.

Benoit, G. and H. F. Hemond (1990). [210]Po and ^{210}Pb remobilization from lake sediments in relation to iron and manganese cyling. *Environ. Sci. Technol. 24*, 1224-1234.

Bertram, M. A. and J. P. Cowen (1997). Morphological and compositional evidence for biotic precipitation of marine barite. *Journal of Marine Research 55*, 577-593.

Canfield, D., W. J. Green and P. Nixon (1995). [210]Pb and stable lead through the redox transition zone of an Antarctic lake. *Geochim. Cosmochim. Acta 59*, 2459-2468.

Carrick, T. R. and D. W. Sutcliffe (1982). Concentrations of major ions in lakes and tarns of the English Lake District (1953-1978). No. 16.

Crowther, D. L., J. G. Dillard and J. W. Murray (1983). The mechanism of Co(II) oxidation on synthetic birnessite. *Geochim. Cosmochim. Acta 47*, 1399-1403.

Davison, W. (1993). Iron and manganese in lakes. *Earth-Sci. Rev. 34*, 119 - 163.

Davison, W., J. Buffle and R. DeVitre (1998). Voltammetric characterization of a dissolved iron sulphide species by laboratory and field studies. *Anal. Chim. Acta 377*, 193-203.

Davison, W., G. W. Grime and C. Woof (1992). Characterization of lacustrine iron sulfide particles with proton-induced X-ray emission. *Limnol. Oceanogr. 37*, 1770-1777.

Davison, W. and S. I. Heaney (1978). Ferrous iron-sulfide interactions in anoxic hypolimnetic waters. *Limnol. Oceanogr. 23*, 1194-1200.

Davison, W., S. I. Heaney, J. F. Talling and E. Rigg (1980). Seasonal transformations and movements of iron in a productive English lake with deep-water anoxia. *Schweiz. Z. Hydrol. 42*, 196-224.

Davison, W. and J. P. Lishman (1983). Rapid colorimetric procedure for the determination of acid volatile sulphide in sediments. *Analyst 108*, 1235-1239.

Davison, W., C. Woof and E. Rigg (1982). The dynamics of iron and manganese in a seasonally anoxic lake; direct measurement of fluxes using sediment traps. *Limnol. Oceanogr. 27*, 987-1003.

Ellwood, M. J., K. A. Hunter and J. P. Kim (2001). Zinc speciation in Lakes Manapouri and Hayes, New Zealand. *Marine and Freshwater Research 52*, 217-222.

Finlay, B. J., N. B. Hetherington and W. Davison (1983). Active biological participation in lacustrine barium chemistry. *Geochim. Cosmochim. Acta 47*, 1325-1329.

Fortin, D., G. G. Leppard and A. Tessier (1993). Characteristics of lacustrine diagenetic iron oxyhydroxides. *Geochim. Cosmochim. Acta 57*, 4391-4404.

Grime, G. W., M. Dawson, M. Marsh, I. C. McArthur and F. Watt (1991). The Oxford submicron nuclear microscopy facility. *Nuclear Instruments and Methods in Physics Research B54*, 52-63.

Hamilton-Taylor, J. and W. Davison (1995). Redox-driven cycling of trace elements in lakes. *Physics and Chemistry of Lakes*. A. Lerman, Imboden, D. & Gat, J., Springer-Verlag: 217-263.

Hamilton-Taylor, J., W. Davison and K. Morfett (1996). The biogeochemical cycling of Zn, Cu, Fe, Mn, and dissolved organic C in a seasonally anoxic lake. *Limnol. Oceanogr. 41*, 408-418.

Hamilton-Taylor, J., W. Davison and K. Morfett (1996). A laboratory study of the biogeochemical cycling of Fe, Mn, Zn and Cu across the sediment-water interface of a productive lake. *Aquatic Sciences 58*, 191-209.

Hamilton-Taylor, J. and E. B. Morris (1985). The dynamics of iron and manganese in the surface sediments of a seasonally anoxic lake. *Archiv für Hydrobiol., Suppl.-Bd. 72*, 135-165.

Hamilton-Taylor, J., E. J. Smith, W. Davison and H. Zhang (1999). A novel DGT-sediment trap device for the in situ measurement of element remobilization from settling particles in water columns and its application to trace metal release from Mn and Fe oxides. *Limnol. Oceanogr. 44*, 1772-1780.

Heaney, S. I., W. J. P. Smyly and J. F. Talling (1986). Interactions of physical, chemical and biological processes in depth and time within a productive English lake during summer stratification. *Internationale Revue der gesamten Hydrogiologie 71*, 441-494.

Honeyman, B. D. and P. H. Santschi (1988). Metals in aquatic systems. *Environ. Sci. Technol. 22*, 862-871.

Honeyman, B. D. and P. H. Santschi (1989). A Brownian-pumpiin model for oceanic trace metal scavenging: Evidence from Th isotopes. *JMR 47*, 951-992.

Huerta-Diaz, M. A., A. Tessier and R. Carignan (1998). Geochemistry of trace metals associated with reduced sulfur in freshwater sediments. *Applied Geochemistry 13*, 213-233.

Jacobs, L. and S. Emerson (1982). Trace metal solubility in an anoxic fjord. *Earth Planet. Sci. Lett. 60*, 237-252.

Jacobs, L., S. Emerson and J. Skei (1985). Partitioning and transport of metals across the O_2/H_2S interface in a permanently anoxic basin: Framvaren Fjord, Norway. *Geochimica et Cosmochimica Acta 49*, 1433-1444.

Kenison Falkner, K., G. P. Klinkhammer, T. S. Bowers, J. F. Todd, B. L. Lewis, W. M. Landing and J. M. Edmond (1993). The behavior of barium in anoxic marine waters. *Geochim. Cosmochim. Acta 57*, 537-554.

Kleeberg, A. and H. Schubert (2000). Vertical gradients in particle distribution and its elemental composition under oxic and anoxic conditions in a eutrophic lake, Scharmutzelsee, NE Germany. *Archiv Fur Hydrobiologie 148*, 187-207.

Kremling, K. (1983). The behavior of Zn, Cd, Cu, Ni, Co, Fe and Mn in anoxic Baltic waters. *Marine Chemistry. 13*, 87-108.

LaZerte, B. D. (1989). Aluminium speciation and organic carbon in waters of central Ontario. *Environmental Chemistry and Toxicity of Aluminium*. T. E. Lewis, Lewis: 195-207.

Lienemann, C. P., M. Taillefert, D. Perret and J. F. Gaillard (1997). Association of cobalt and manganese in aquatic systems: Chemical and microscopic evidence. *Geochimica Et Cosmochimica Acta 61*, 1437-1446.

Lofts, S. and E. Tipping (1998). An assemblage model for cation binding by natural particulate matter. *Geochimica Et Cosmochimica Acta 62*, 2609-2625.

Lofts, S. and E. Tipping (2001). WHAM6. Windermere Humic Aqueous Model. Equilibrium chemical speciation for natural waters., Natural Environment Research Council.

Loganathan, P. and R. G. Burau (1973). Sorption of heavy metal ions by a hydrous manganese oxide. *Geochim. Cosmochim. Acta 37*, 1277-1293.

Maberley, S. C. (1996). Diel, episodic and seasonal changes in pH and concentrations of inorganic carbon in a productive lake. *Freshwater Biology 35*, 579-598.

Malcolm, R. L. (1985). Geochemistry of stream fulvic and humic substances. *Humic Substances in Soil, Sediment, and Water.* G. R. Aiken, D. M. Mcknight and R. L. Wershaw, Wiley-Interscience: 181-209.

McGrath, M., W. Davison and J. Hamilton-Taylor (1989). Biogeochemistry of barium and strontium in a softwater lake. *Sci. Tot. Environ. 87/88*, 287-295.

Michard, G., E. Viollier, D. Jezequel and G. Sarazin (1994). Geochemical study of a crater lake - Pavin Lake, France - Identification, location and quantification of the chemical reactions in the lake. *Chem. Geol. 115*, 103-115.

Morse, J. W. and T. Arakaki (1993). Adsorption and coprecipitation of divalent metals with mackinawite (FeS). *Geochim. Cosmochim. Acta 57*, 3635-3640.

NIST (1997). Critically Selected Stability Constants of Metal Complexes Database, version 4.0., US Department of Commerce.

Rickard, D. (1989). Experimental concentration-time curves for the iron(II) sulphide precipitation process in aqueous solutions and their interpretation. *Chem. Geol. 78*, 315-324.

Sholkovitz, E. R. (1985). Redox-related geochemistry in lakes; alkali metals, alkaline earth metals, and ^{137}Cs. *Chemical Processes in Lakes.* W. Stumm. New York, Wiley: 119-142.

Sholkovitz, E. R. and D. Copland (1982). The chemistry of suspended matter in Esthwaite Water, a biologically productive lake with seasonally anoxic hypolimnion. *Geochim. Cosmochim. Acta. 46*, 393-410.

Sigg, L., A. Kuhn, H. B. Xue, E. Kiefer and D. Kistler (1995). Cycles Of Trace-Elements (Copper and Zinc) In a Eutrophic Lake - Role Of Speciation and Sedimentation. *Advances In Chemistry Series 244*, 177-194.

Smith, E. J. (1998). The biogeochemical behaviour of trace metals in a seasonally anoxic lake., University of Lancaster: 306.

Smith, E. J., N. Phillips, J. Hamilton-Taylor, W. Davison, C. P. Murdock, M. Kelly and B. Tabner (1996). The behaviour of Cu, Pb-210 and Po-210 in the water column of a productive lake during seasonal anoxia. Proc. Fourth Internat. Symp. on Geochemistry of the Earth's Surface, Ilkley, UK.

Smith, R. M. and A. E. Martell (1976). Critical Stability Constants. Vol. 4. Inorganic Complexes. New York, Plenum Press.

Stroobants, N., F. Dehairs, L. Goeyens, N. Vanderheijden and R. van Grieken (1991). Barite Formation in the Southern-Ocean Water Column. *Marine Chemistry 35*, 411-421.

Stumm, W. and J. J. Morgan (1996). Aquatic Chemistry. New York, Wiley.

Sugiyama, M. and T. Hori (1994). Geochemical behaviour of barium in the vicinity of a MnO_2/Mn^{2+} redox front formed in a eutrophic lake. *Jpn. J. Limnol. 55*, 27-37.

Sugiyama, M., T. Hori, S. Kihara and M. Matsui (1992). A geochemical study on the specific distribution of barium in Lake Biwa, Japan. *Geochim. Cosmochim. Acta 56*, 597-605.

Sutcliffe, D. W., Carrick, T. R., Heron, J., Rigg, E., Talling, J. F., Woof, C. & Lund, J. W. G. (1982). Long-term and seasonal changes in the chemical composition of precipitation and surface waters of lakes and tarns in the English Lake District. *Freshwater Biology 12*, 451-506.

Taillefert, M., C. P. Lienemann, J. F. Gaillard and D. Perret (2000). Speciation, reactivity, and cycling of Fe and Pb in a meromictic lake. *Geochimica Et Cosmochimica Acta 64*, 169-183.

Taillefert, M., B. J. MacGregor, J. F. Gaillard, C. P. Lienemann, D. Perret and D. A. Stahl (2002). Evidence for a dynamic cycle between Mn and Co in the water column of a stratified lake. *Environmental Science & Technology 36*, 468-476.

Tipping, E. (1994). WHAM- a chemical equilibrium model and computer code for waters, sediments, and soils incorporating a discrete site/electrostatic model of ion binding by humic-substances. *Computers and Geosciences 20*, 973-1023.

Tipping, E. (1998). Humic ion-binding Model VI: an improved description of the interactions of protons and metal ions with humic substances. *Aquat. Geochem. 4*, 3-48.

Tipping, E., N. B. Hetherington, J. Hilton, D. W. Thompson, E. Bowles and J. Hamilton-Taylor (1985). Artifacts in the use of selective chemical extraction to determine distributions of metals between oxides on Mn and Fe. *Analytical Chemistry 57*, 1944-1946.

Tipping, E., C. Rey-Castro, S. E. Bryan and J. Hamilton-Taylor (2002). Al(III) and Fe(III) binding by humic substances in freshwaters, and implications for trace metal speciation. *Geochim. Cosmochim. Acta 66*, 3211-3224.

Tipping, E., D. W. Thompson and W. Davison (1984). Oxidation products of Mn(II) in lake waters. *Chem. Geol. 44*, 359-383.

Tipping, E. and C. Woof (1983). Seasonal-Variations in the Concentrations of Humic Substances in a Soft-Water Lake. *Limnology and Oceanography 28*, 168-172.

Tipping, E., C. Woof and D. Cooke (1981). Iron oxide from a seasonally anoxic lake. *Geochim. Cosmochim. Acta 45*, 1411-1419.

Viollier, E., D. Jezequel, G. Michard, M. Pepe, G. Sarazin and P. Alberic (1995). Geochemical study of a crater lake (Pavin Lake, France): Trace-element behaviour in the monimolimnion. *Chem. Geol. 125*, 61-72.

Viollier, E., G. Michard, D. Jezequel, M. Pepe and G. Sarazin (1997). Geochemical study of a crater lake: Lake Pavin, Puy de Dome, France. Constraints afforded by the particulate matter distribution in the element cycling within the lake. *Chemical Geology 142*, 225-241.

Xue, H. B., R. Gachter and L. Sigg (1997). Comparison of Cu and Zn cycling in eutrophic lakes with oxic and anoxic hypolimnion. *Aquatic Sciences 59*, 176-189.

TABLES

Table 1. Analytical techniques and performance data for dissolved metal analysis**.**

Metal	Technique	Analytical Precision [a]	D.L.[b] nM	Field Blank nM
Mn	GF-AAS	$\pm\,2\%$	2.82	5.37
Fe	GF-AAS	$\pm\,2\%$	18.6	< D.L.
Co	ICPMS	$\pm\,2\%$	0.16	< D.L.
Al	ICPMS	$\pm\,5\,\%$	1.70	5.45
Ba	ICPMS	$\pm\,0.4\,\%$	0.15	0.59
Ni	ICPMS	$\pm\,5\,\%$	1.84	< D.L.
Cu	ICPMS	$\pm\,5\,\%$	2.13	< D.L.
Pb	ICPMS	$\pm\,6\,\%$	0.80	< D.L.

(a) Overall mean value of $100(\sigma/\bar{x})$, where $\sigma/\bar{x}$ is based on routine triplicate subsampling and analysis.

(b) Analytical Detection Limit = 3σ of 15 MQ blanks.

Table 2. Solution conditions used to calculate equilibrium speciation.

	Metalimnion	Epilimnion
Temperature (°C)	15	20
Na (M)	2.5×10^{-4}	2.5×10^{-4}
K (M)	2.5×10^{-5}	2.5×10^{-5}
Ca (M)	2.6×10^{-4}	2.6×10^{-4}
Mg (M)	6.6×10^{-5}	6.6×10^{-5}
Cl (M)	2.4×10^{-4}	2.4×10^{-4}
SO_4 (M)	1.2×10^{-4}	1.2×10^{-4}
NO_3 (M)	0	0
pH	7	8, 9
P_{CO_2} (atmos.)	1.65×10^{-3}	2.4×10^{-4}, 2.2×10^{-5}
Alkalinity[a] (μequiv L^{-1})	300	400, 410
Dissolved fulvic acid (mg L^{-1})	1, 2	1, 2
$a_{Fe^{3+}}$ (M)	1×10^{-17}	1×10^{-20}, 1×10^{-23}
FeOOH (μg L^{-1})	62, 2700	62
MnO_2 (μg L^{-1})	44	44
Particulate fulvic acid (μg L^{-1})[b]	7, 300	7
Total Al (nM)	150	150
Total Co (nM)	2	2
Total Ni (nM)	8	8
Total Cu (nM)	10	10
Total Ba (nM)	90	90
Total Pb (nM)	4	4

(a) Calculated using WHAM6.

(b) Associated predominantly with Fe oxide

Table 3. Pearson correlation coefficients between dissolved and labile particulate Mn, Fe and trace metals in the water column above 10 m depth for 22nd August 1996.

	Mn		Fe	
	Dissolved 6 - 10 m n = 5	Particulate 3 - 10 m n = 8	Dissolved 6 - 10 m n = 5	Particulate 3 - 10 m n = 8
Mn	-	-	0.90**	-0.09
Co	0.98**	0.22	0.92**	0.58
Al	0.98**	-	0.87**	-
Ba	0.98**	0.96**	0.97**	0.12
Ni	0.97**	0.72*	0.83*	-0.21
Cu	0.24	-	-0.01	-
Pb	0.47	-	0.23	-

** Significant at 99% confidence level.

* Significant at 95% confidence level.

Table 4. Comparison of metal:Mn molar ratios derived from DGT-trap remobilization measurements (Hamilton-Taylor et al. 1999) with those from regression analysis of water column concentrations in the depth zone of Mn-oxide redox cycling in Esthwaite Water.

	Aug 1996 Trap derived ratio / 10^{-3}	Aug 22, 1996 Regression of dissolved metal[a] / 10^{-3}	Aug 22, 1996 Regression of labile particulate metal[b] / 10^{-3}	Aug 1997 Trap derived ratio / 10^{-3}
Co	0.27	0.29	not significant	0.26
Al	1.26	2.42	-	3.83
Ba	0.66	2.77	13.7	0.62
Ni	0.08	0.18	1.9	3.20

(a) Based on concentrations at 6-10 m depth.

(b) Based on concentrations at 3-10 m depth.

Table 5. Pearson correlation coefficients between dissolved and labile particulate Mn, Fe and trace metals in the water column below 10 m depth for 22nd August 1996.

| | Mn | | Fe | |
	Dissolved 10 - 15 m n = 6	Particulate 10 - 15 m n = 6	Dissolved 10 - 15 m n = 6	Particulate 10 - 15 m n = 6
Mn	-	-	-0.84**	0.94**
Co	0.92**	0.88**	-0.83**	0.97**
Al	-0.82*	-	0.98**	-
Ba	-0.86**	0.87**	0.94**	0.93**
Ni	0.79*	0.98**	-0.55	0.98**
Cu	0.74*	0.75*	-0.43	0.84**
Pb	0.63	0.98**	-0.17	0.97**

** Significant at 99% confidence level.

* Significant at 95% confidence level.

Table 6. The metal fractions in various forms predicted by WHAM6 at 2 mg L^{-1} fulvic acid (FA) and 44 µg L^{-1} MnO$_2$ (0.5 µM Mn), as a function of pH and Fe oxide concentration. The sum of the fractions is unity for each metal and the total concentrations are 2 nM Co, 8 nM Ni, 90 nM Ba, 150 nM Al, 4 nM Pb and 10 nM Cu.

Metal	pH	[Fe oxide] (µM)	True Solution[a]	Colloidal FA	Particulate FA[b]	Fe oxide[c]	Mn oxide[c]
Co	7	0.7	0.78	0.04	1.3E-04	8.9E-04	0.19
	8	0.7	0.82	0.04	1.4E-04	4.9E-03	0.14
	9	0.7	0.92	0.02	7.5E-05	7.5E-03	0.05
	7	30	0.75	0.03	5.1E-03	0.03	0.18
Ni	7	0.7	0.89	0.10	3.6E-04	1.2E-03	8.1E-03
	8	0.7	0.89	0.10	3.5E-04	5.2E-03	4.8E-03
	9	0.7	0.95	0.04	1.4E-04	5.8E-03	1.3E-03
	7	30	0.85	0.09	0.01	0.04	7.4E-03
Ba	7	0.7	0.99	7.3E-03	2.6E-05	6.6E-07	1.0E-04
	8	0.7	0.99	7.1E-03	2.5E-05	4.9E-06	1.1E-04
	9	0.7	0.99	6.7E-03	2.4E-05	2.0E-05	1.1E-04
	7	30	0.99	7.3E-03	1.1E-03	2.5E-05	1.0E-04
Al	7	0.7	0.05	0.94	3.3E-03	9.6E-04	1.4E-03
	8	0.7	0.89	0.11	4.0E-04	5.9E-05	7.0E-06
	9	0.7	1.00	0.01	1.8E-05	2.6E-07	7.9E-09
	7	30	0.04	0.81	0.12	0.03	9.8E-04
Pb	7	0.7	2.3E-03	0.16	5.7E-04	0.03	0.80
	8	0.7	5.8E-03	0.59	2.1E-03	0.17	0.24
	9	0.7	3.6E-03	0.79	2.8E-03	0.17	0.02
	7	30	9.6E-04	0.08	0.01	0.56	0.34
Cu	7	0.7	4.8E-03	0.99	3.5E-03	3.5E-04	9.5E-05
	8	0.7	1.1E-03	0.99	3.5E-03	6.3E-04	8.2E-06
	9	0.7	6.0E-04	1.00	3.5E-03	8.0E-04	1.1E-06
	7	30	3.7E-03	0.86	0.13	0.01	7.5E-05

[a] based on free metal ion plus inorganic complexes
[b] based on combined humic contents of both Fe and Mn oxides
[c] based on contents of the pure metal oxides

Table 7. Assumed M_{FeS} and M_b values used in K_d simulations (see text for full explanation).

	Mn/µM	Ba/nM	Co/nM	Cu/nM	Ni/nM
M_{FeS}	0.4	15	6	4	5
M_b	56.6	325	6	1	5

Table 8. Calculated ion activity products (IAP $= a_{Al^{3+}} / a_{H^+}^3$) for Al(OH)$_3$.

Region of water column	pH	[Al$_{total}$] (nM)	fulvic acid (mg L^{-1})	$a_{Al^{3+}}$ (M)	Log$_{10}$ IAP
Epilimnion	8	150	1.5	6.8E-17	7.8
Epilimnion	8	40	1.5	1.7E-17	7.2
Epilimnion	9	150	1.5	7.4E-21	6.9
Epilimnion	9	40	1.5	2.0E-21	6.3
Metalimnion	6.8	40	1.5	5.1E-14	7.1
Hypolimnion	6.8	300	3.0	1.5E-12	8.6

FIGURE LEGENDS

Fig. 1. Vertical profiles of temperature, dissolved oxygen and dissolved sulfide in Esthwaite Water during summer stratification, 1996. The sulfide profile shown for August 22 was actually obtained on August 28.
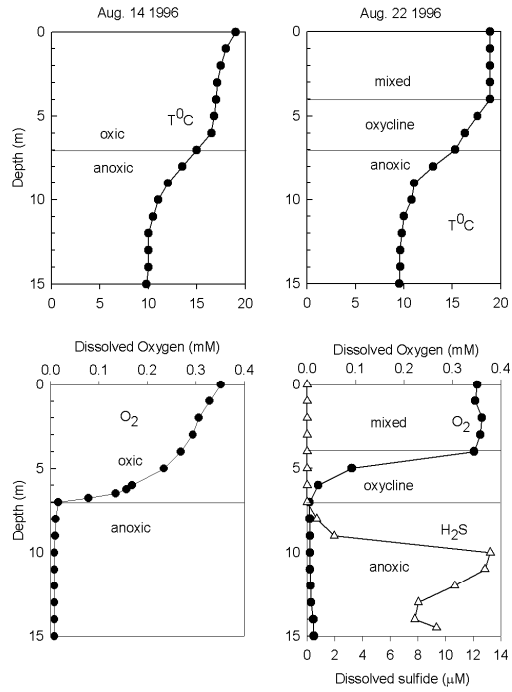
Fig. 2. Vertical profiles of dissolved and labile particulate Mn and Fe in Esthwaite Water during summer stratification, 1996. Particulate concentrations are indicated by open triangles and have a different scale.
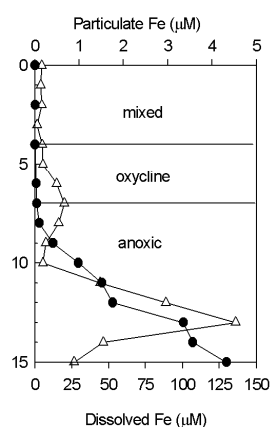
Fig. 3. Vertical profiles of dissolved and labile particulate Co and Ni in Esthwaite Water during summer stratification, 1996. Particulate concentrations are indicated by open triangles and have a different scale.
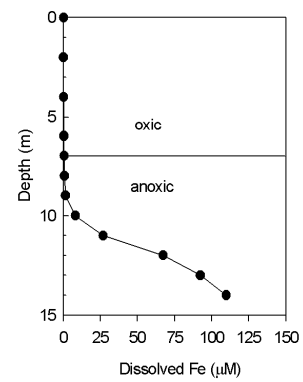
Fig. 4. Vertical profiles of dissolved and labile particulate Ba and Al in Esthwaite Water during summer stratification, 1996. Particulate concentrations are indicated by open triangles and have a different scale.
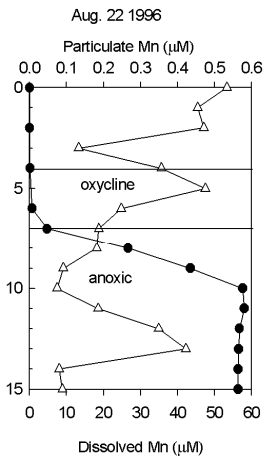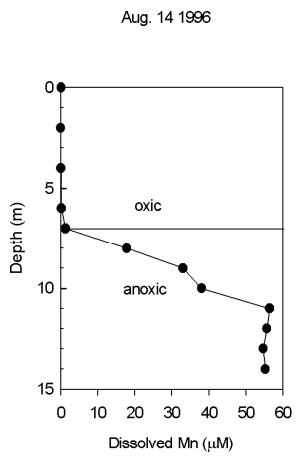
Fig. 5. Vertical profiles of dissolved and labile particulate Pb and Cu in Esthwaite Water during summer stratification, 1996. Particulate concentrations are indicated by open triangles and for Pb have a different scale.

Fig. 6. K_d values for water depths between 10 and 15 m in Esthwaite Water on August 22 1996: (a) observed K_d against dissolved metal concentration, (b) simulated K_d against dissolved metal concentration, and (c) observed K_d against particulate (filterable) FeS concentration.

Aug. 14 1996

Aug. 22 1996

Depth (m)

oxic

anoxic

T^0C

mixed

oxycline

anoxic

T^0C

Dissolved Oxygen (mM)

Dissolved Oxygen (mM)

Depth (m)

O_2

oxic

anoxic

mixed

oxycline

anoxic

O_2

H_2S

Dissolved sulfide (μM)

Aug. 14 1996

Aug. 22 1996

Particulate Mn (μM)

oxic

anoxic

oxycline

anoxic

Dissolved Mn (μM)

Depth (m)

Particulate Fe (μM)

oxic

anoxic

mixed

oxycline

anoxic

Dissolved Fe (μM)

Depth (m)

Aug. 14 1996

Aug. 22 1996

Particulate Co (nM)

Depth (m)

oxic

anoxic

Dissolved Co (nM)

mixed

oxycline

anoxic

Dissolved Co (nM)

Particulate Ni (nM)

Depth (m)

oxic

anoxic

Dissolved Ni (nM)

mixed

oxycline

anoxic

Dissolved Ni (nM)

Aug. 14 1996

Aug. 22 1996

Particulate Ba (nM)

Dissolved Ba (nM)

Depth (m)

oxic

anoxic

mixed

oxycline

anoxic

Dissolved Al (nM)

oxic

anoxic

mixed

oxycline

anoxic